A Facile Route To Recover Intrinsic Graphene over Large Scale

Dong-Wook Shin,[†] Hyun Myoung Lee,[‡] Seong Man Yu,[†] Kwang-Soo Lim,[†] Jae Hoon Jung,[‡] Min-Kyu Kim,[†] Sang-Woo Kim,[†,‡] Jae-Hee Han,[§] Rodney S. Ruoff,[†,∥] and Ji-Beom Yoo[†,‡,*]

[†]SKKU Advanced Institute of Nanotechnology (SAINT), and [‡]School of Advanced Materials Science and Engineering (BK21), Sungkyunkwan University, 300, Chunchun-dong, Jangan-gu, Suwon, 440746, Republic of Korea, [§]Department of Energy IT, Gachon University, Seongnam, Gyeonggi-do, 461701, Republic of Korea, and [∥]Department of Mechanical Engineering and the Materials Science and Engineering Program, The University of Texas, Austin, Texas, United States

ABSTRACT

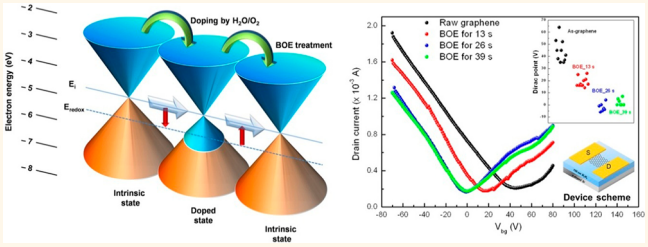

The intrinsic properties of initially p-type doped graphene (grown by chemical vapor deposition (CVD)) can be recovered by buffered oxide etch (BOE) treatment, and the dominant factor governing p-type doping is identified as the H_2O/O_2 redox system. Semi-ionic C—F bonding prevents the reaction between the products of the H_2O/O_2 redox system and graphene. BOE-treated graphene field effect transistors (FETs) subsequently exposed to air, became p-type doped due to recovery of the H_2O/O_2 redox system. In comparison, poly(methyl methacrylate) (PMMA)-coated graphene FETs had improved stability for maintaining the intrinsic graphene electronic properties.

KEYWORDS: graphene · transistor · intrinsic properties · buffed oxide etch (BOE) · PMMA · H_2O/O_2 redox system · Fermi level

Graphene is ambipolar with a zero neutrality point in field effect transistors (FETs, *i.e.*, graphene FETs (GFETs)). The electronic structure of graphene is modified by adsorbates,[1] and n- and p-type GFETs have been thereby made.[1−5] However, during transfer of graphene and fabrication of GFETs, some adsorbates are unintentionally adsorbed typically yielding p-type doped graphene. Several mechanisms for the p-type doping of graphene by unwanted adsorbates have been proposed, including charge transfer doping from H_2O/O_2 molecules[6,7] and the enhancement of external scattering centers by residues from, for example, poly(methyl methacrylate) (PMMA).[8−11] Is the dominant doping of graphene in, for instance, GFETs by H_2O/O_2 molecules or residues such as PMMA on the graphene, or both? Another important issue is the repeatability and performance of electronic devices using unintentionally doped graphene. It is important to be able to restore the intrinsic properties, $V_{dirac} \approx 0$, of GFETs, and to this end thermal treatment in high vacuum systems[8−10] and wet treatments such as with chloroform[11] have been used; these approaches have focused on the removal of resist residues such as PMMA to recover intrinsic graphene response. We estimated the reason of dominant doping of graphene through the studies of p-type doped single walled carbon nanotube (SWCNT) FET in the environment.[12−14] SWCNTs have a similar reaction with adsorbates in the environment as graphene, resulting in p-type doped properties due to the water and/or oxygen molecules.[12−14] The studies of SWCNT doping can help to understand the dominant factor governing the mechanism of the initially p-doped graphene.

Here graphene synthesized by CVD on Cu foil was treated with buffered oxide etch (BOE), and it was learned that this recovers intrinsic graphene. A mechanism by which the intrinsic properties of initially p-type doped graphene can be recovered is presented, and the dominant factor governing this process is identified. GFETs based on an Si_3N_4 dielectric layer were treated with a BOE solution, which was used several times for the removal of native oxides and to etch the nitride layer for making a suspended structure.[15,16] The BOE treatment of graphene eliminates the H_2O/O_2 redox system due to the reaction between HF and H_2O. By study of GFETs having residual PMMA and also PMMA-coated GFETs, it was found that the dominant factor for p-doping was electron transfer by the H_2O/O_2 redox system. A substantial improvement in stability of the intrinsic properties of graphene in an air is obtained by PMMA coating of GFETs.

* Address correspondence to jbyoo@skku.edu.

Received for review April 22, 2012 and accepted August 28, 2012.

Published online 10.1021/nn3017603

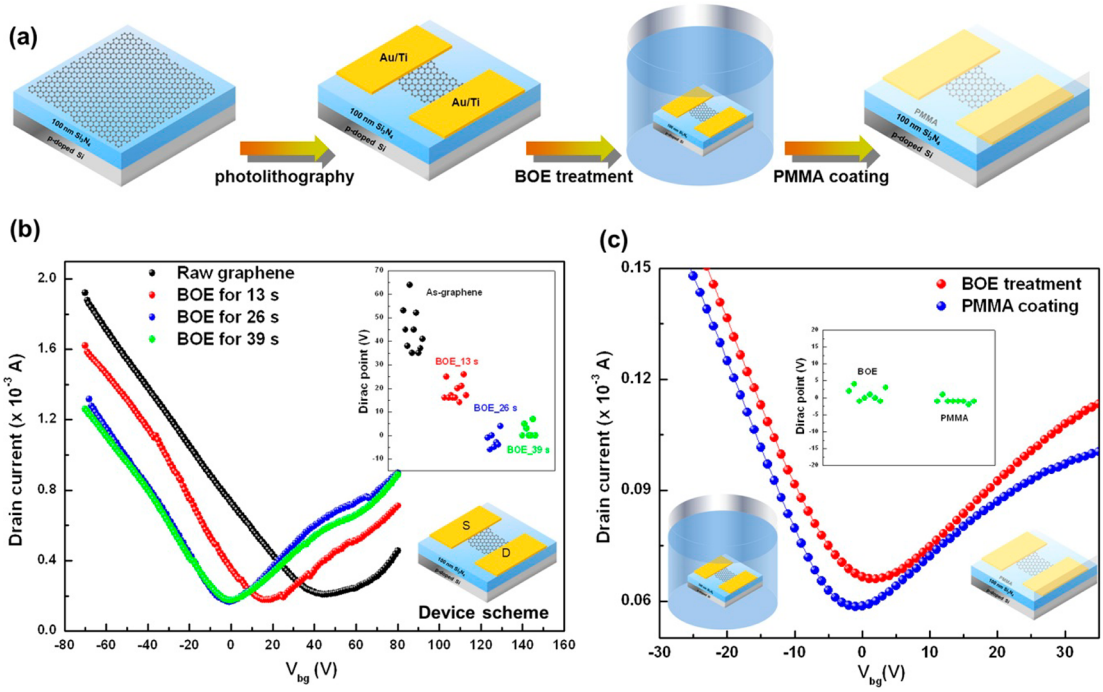

Figure 1. Schematic of the BOE treatment methods and the transfer characteristics of graphene-Si_3N_4 FETs. (a) After making GFETs, they were treated with BOE solution, and then coated with PMMA. (b) GFETs before and after BOE treatment in ambient conditions. (c) BOE-treated GFETs (red dots) and PMMA-coated GFET (blue dots) made according to panel a. The inset image and graph (b and c) are the device schematic and variation of V_{dirac}, respectively.

RESULTS AND DISCUSSIONS

Graphene in the GFETs was treated with BOE solution according to the method as shown in Figure 1a: after making the GFETs on a gate insulator of Si_3N_4, they were dipped in BOE solution for different exposure times, and then coated with PMMA. The electrode of a source-drain (S-D) in GFET was the metal configuration of Ti and Au as shown in Figure 1a. As the same contact metal configuration was used for all the devices used in this work, a variation in the work function of contact metal that would dope graphene can be excluded.[6,14] The electronic response of the aforementioned GFETs is shown in Figure 1b,c. The device structure and the movement of a Dirac point (V_{dirac}) are shown in the inset of Figure 1b,c. As the exposure to BOE increases up to 26 s (Figure 1b), the V_{dirac} shifted from ~45 to ~0 V. Further BOE treatment of GFETs (39 s) resulted in negligible change in the V_{dirac}. Although residual PMMA remained on the graphene surface during the PMMA coating process (explained in detail in Figure 3), V_{dirac} values for GFETs were ~0 V. Figure 1c shows that BOE-treated GFETs (red dots) and PMMA-coated GFETs (blue dots) have a V_{dirac} value of ~0 V. Schematics of the exposure to the BOE solution, and the device, are shown in Figure 1c. The BOE recovers the intrinsic properties of graphene. We have investigated the GFETs in an attempt to identify the effect of residues on the graphene surface. The residual PMMA and/or PMMA film also did not have any effect on the electronic properties of graphene because those GFETs had a Dirac point of ~0 V. The dominant factor in restoring the Fermi level of graphene to the intrinsic energy level, E_i, is thus the removal of the interaction of the H_2O/O_2 redox system and graphene, not the removal of the residual PMMA.

From the analysis of the intensity, frequency, and position of the characteristic G-, D-, and 2D-Raman modes, the crystalline quality, doping level, and strain were evaluated at different locations on the graphene. The Si_3N_4 layer thickness was controlled by BOE treatment in order to obtain high optical contrast for graphene based on the optical reflection and transmission between it and the Si_3N_4 layer.[17,18] An 82 nm thick Si_3N_4 layer was selected to obtain high intensity signals in the Raman spectra. Figure 2 shows the Raman spectra of as-prepared graphene and BOE-treated graphene at the 633 nm excitation wavelength. For 13 s of treatment, the position of the G-band was shifted from ~1590 to ~1586 cm^{-1}, Figure 2b. However, as the BOE treatment time increases above 13 s, the G-band did not shift further. The 2D band (Figure 2c) was slightly red-shifted from ~2649 to ~2645 cm^{-1} for the 13 s BOE exposure. For treatment times of more than 13 s, the 2D did not further shift. No enhancement of the D-band was observed (Figure 2a). These results indicate that the positions of the G- and 2D bands of graphene on Si_3N_4 are red-shifted when doping is eliminated by the BOE treatment; since the D-band does not change we infer that there is no chemistry, or at least no substantial chemical change,

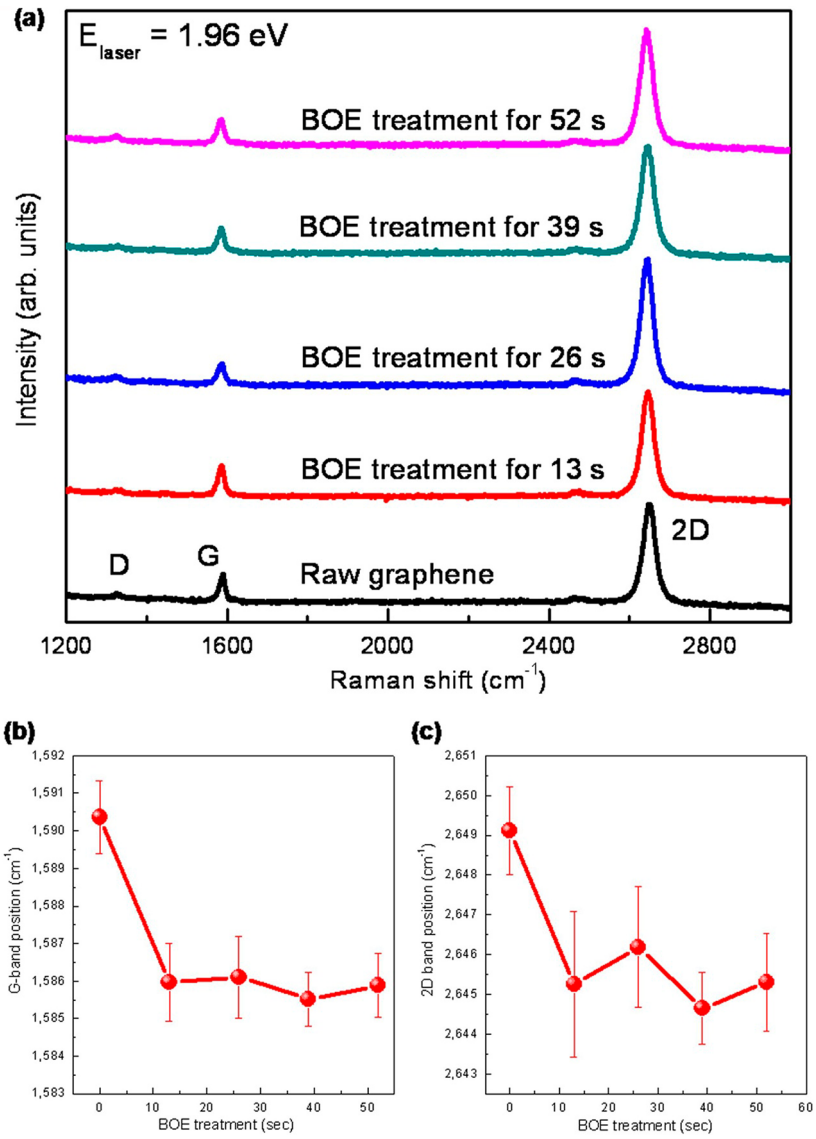

Figure 2. Raman spectra of graphene treated with BOE: (a) Raman spectra of graphene treated by BOE for various times (0 to 52 s); (b) variation of G-band position and (c) 2D band position with increasing BOE treatment time.

from exposure to BOE. We infer that the interaction between the H_2O/O_2 redox system and graphene is removed by BOE treatment without any change in the graphene structure.

Figure 3 shows XPS spectra of C 1s, O 1s, and F 1s of graphene before and after BOE treatment for 13 s. According to the XPS spectra of C 1s (Figure 3a), as-prepared graphene showed the C−C carbon group and the residual PMMA on the graphene surface, consistent with previous work.[19,20] After BOE treatment of graphene on Si_3N_4, no changes in these peak positions and no new functional groups were found, Figure 3d, indicating no change in the covalent chemical bonding networks and removal of residual PMMA in graphene from the BOE treatment. Changes in the XPS spectra of O 1s and F 1s in the graphene film on Si_3N_4 were observed after the BOE treatment. In Figure 3b, an O 1s peak at 532.5 eV is seen, and is due to a layer of H_2O[21−23] adsorbed onto the Si_3N_4 dielectric. The Si_3N_4 dielectric layer has a very thin H_2O layer because the Si_3N_4 surface has imino (NH) groups that adsorb the water molecules through hydrogen-bonding.[24,25] In the studies of SWCNT and graphene FET on SiO_2, a very thin H_2O layer was observed on the hydrophilic oxide layer (SiO_2).[6,14] After BOE treatment, the intensity of the 532.5 eV peak decreased but the 534.2 eV peak intensity increased, Figure 3e. For the F 1s region, Figure 3c, the ionic C−F bonding peak was barely seen before BOE treatment, indicating a concentration of such F-bonded species under 0.2 atom %. After BOE treatment, peaks at 686.7 and 689.3 eV were observed, Figure 3f, and were assigned to Si−F bonding[26] and semi-ionic fluorine,[27] respectively, according to HF (aq) + H_2O (l) ↔ F^- + H_3O^+. We suggest that H_3O^+ is related to the 534.2 eV O 1s peak, Figure 3e. In Figure 3b, the 534.2 eV peak might be present because of dilute hydrochloric acid used

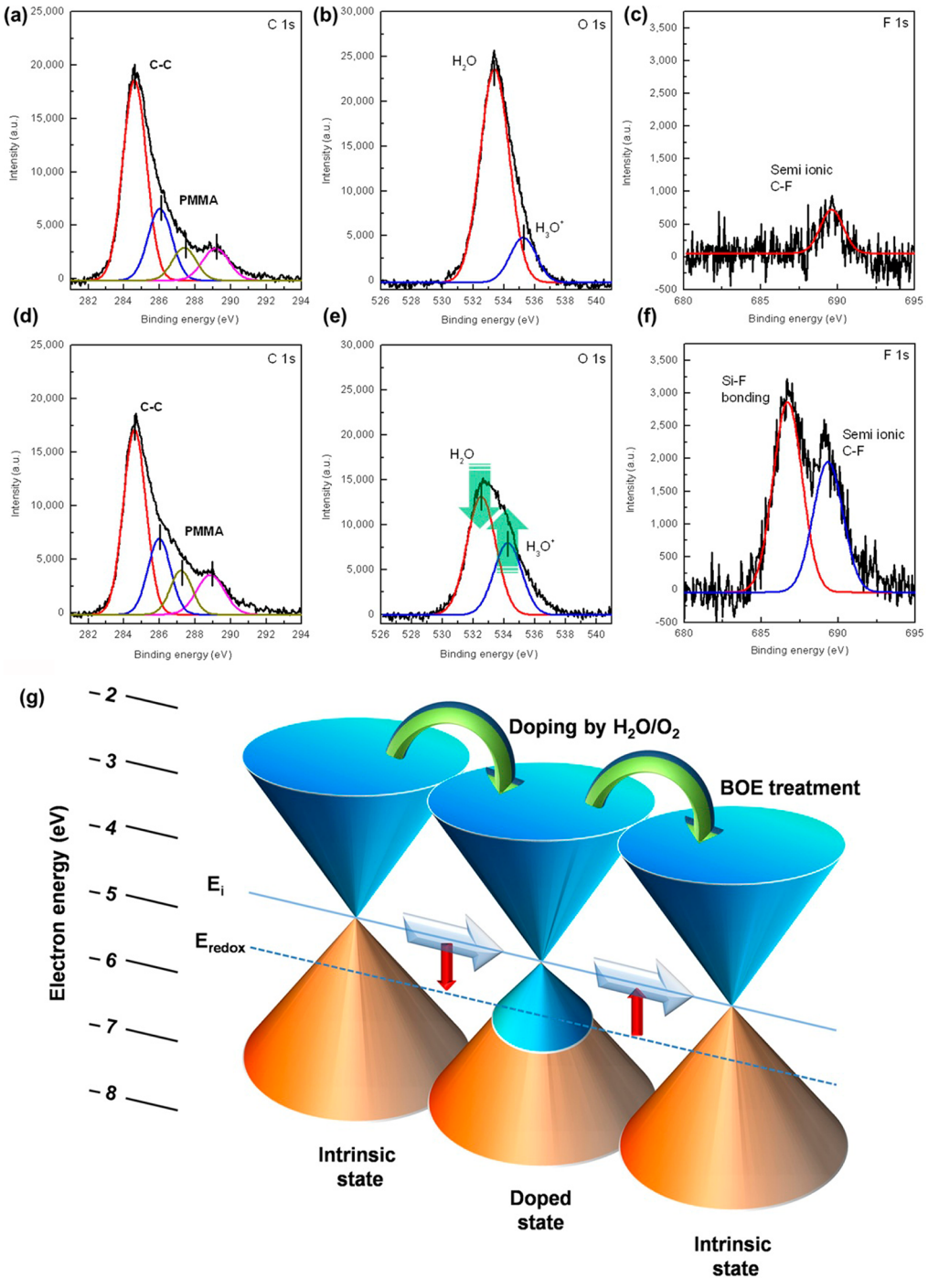

Figure 3. XPS spectra of graphene before and after BOE treatment and scheme of charge transfer between H_2O/O_2 and graphene. C 1s, O 1s, and F 1s in graphene layer before (a, b, and c) and after (d, e, and f) BOE treatment, respectively. After BOE treatment, the peaks in the O 1s and F 1s regions changed due to the chemical reaction of HF (aq) + H_2O (l) ↔ F^- + H_3O^+. (g) The change in the Fermi level of graphene induced by the effect of H_2O/O_2 molecules (doped state) and BOE treatment (intrinsic state). Fermi level of electrons in the H_2O/O_2 redox system, E_{redox}, and graphene is −5.3 and ~4.6 eV, respectively. The difference of Fermi level of H_2O/O_2 redox system and graphene provides a strong driving force for charge transfer. Semi-ionic C−F and Si−F bonding of graphene plays a role in the recovery of the intrinsic graphene properties.

during the transfer of graphene from the copper foil onto the Si_3N_4. The graphene layer is likely to form semi-ionic bonds with F^- ions because graphene has a net positive charge (explained in detail in Figure 3g); and if this is the case, the graphene layer is passivated and the reaction between the H_2O/O_2 redox system and graphene is eliminated. Si−F bonds formed on the Si_3N_4 dielectric layer by the BOE treatment also play a role in preventing the interaction of the H_2O/O_2 redox system and graphene. Therefore, we propose that the intrinsic electrical properties of graphene are recovered because of Si−F and C−F bonds due to the BOE treatment.

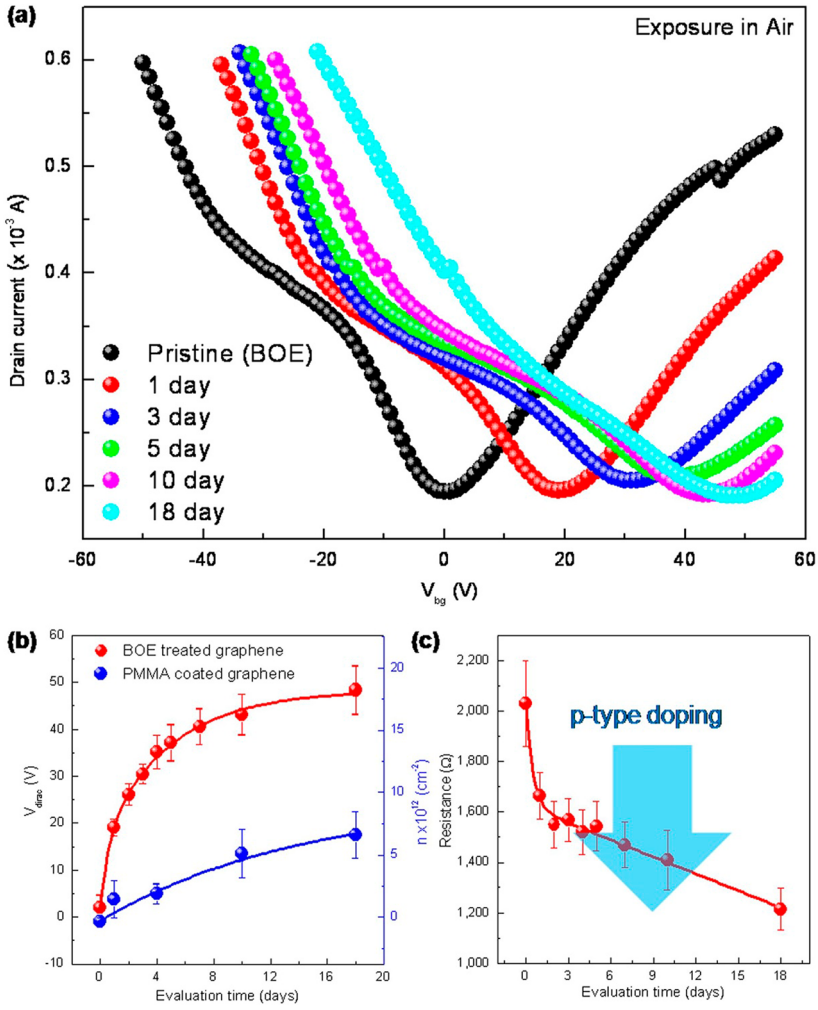

Figure 4. Time evaluation of graphene FET based on the gate insulator of Si_3N_4 exposed in an air for various days. BOE-treated GFETs were exposed in ambient condition for days. PMMA was coated on BOE-treated GFETs. (a) Transfer characteristics of GFET exposed to air for days. (b) The change of V_{dirac} (left) and net charge density (right) of BOE-treated GFETs and PMMA-coated GFETs. The lines are a guide for the eye only. (c) The variation of resistance, R_{SD}, of BOE-treated graphene.

As described in the previous reports on O_2/water mediated surface charge transfer to explain the p-doping of SWCNT and diamaond,[14,28] water supplies solvated O_2 to the graphene electrode, which sets the conditions for the redox reaction.[6] Water in equilibrium with air has pH ≈ 6 from the CO_2 in the air.[28]

The reaction,

$$O_2 + 4H^+ + 4e^-(\text{graphene}) \overset{\text{redox}}{\longleftrightarrow} 2H_2O \qquad (1)$$

dominates under acidic conditions.

The reaction thermodynamics in eq 1 are influenced by the H_2O/O_2 system and its acidity.[28] The redox potential, E_{redox}, of electrons in the H_2O/O_2 redox system is given by the Nernst equation.[6,28]

$$E_{redox} = \mu_{e(SHE)} + E^0_{redox} + \frac{aRT}{n_eF}[4pH - \log(c_{ox})] \qquad (2)$$

where $\mu_{e(SHE)} = -4.44$ eV is the standard hydrogen electrode (SHE) potential relative to the vacuum level, E^0_{redox} is the standard electrode potential of this reaction *versus* the SHE, F is the Faraday constant, n_e is the number of moles of electrons, R is the ideal gas constant, $(aRT/(n_eF)) = 0.0592/4$ eV (at $T = 298$ K), and c_{ox} is the oxygen concentration. So, the E_{redox} of electrons in the H_2O/O_2 redox system is -5.3 eV at pH ≈ 6. The Fermi level of graphene is ~4.6 eV.[29] The Fermi level of graphene lies above the electrochemical potential of the H_2O/O_2 redox system, Figure 3g, which provides a strong driving force to shift the Fermi level of graphene toward that of the H_2O/O_2 redox system at equilibrium. O_2 molecules solvated in the water layer adsorbed on Si_3N_4 obtain $4e^-$ from the graphene and are involved in up to four intermediate reactions in eq 1, generating highly reactive species such as the superoxide anion ($O_2^{\bullet -}$), peroxide (H_2O_2), and hydroxyl radical ($^{\bullet}OH$).[30] These strong Brønsted bases can form "traps" at the Si_3N_4 surface that fix a net negative charge. That stabilizes a net positive charge (hole) in the graphene layer, which explains the positive shift of the V_{dirac} of graphene in Figure 1c.[6] So, the graphene

on the dielectric layer of Si_3N_4 was initially p-doped, Figure 3g. Similarly, the electrons in the SWCNT on SiO_2 readily transfer from the semiconducting carbon nanotubes to H_2O/O_2 redox system due to the difference of the Fermi energy between the SWCNT and H_2O/O_2 redox system, resulting in the unipolar p-type conduction behavior of SWCNT.[14] Thus, the dominant factor governing the mechanism of the initially p-doped graphene was H_2O/O_2 redox system on a hydrophilic dielectric layer (Si_3N_4). As the graphene is exposed to the BOE solution, HF (a weak acid in water) is partially deprotonated by the water layer that is between the graphene and the Si_3N_4, according to the Brønsted-Lowry definition, and F^- and H_3O^+ ions are formed. Although only a small fraction ($\sim$ 2.5%) of the HF molecules are theoretically dissociated to ions in bulk H_2O, once the F^- is "trapped" in an ionic bond with the positively charged graphene, Le Chatelier's principle would show that further dissociation of HF to form F^- would be expected, until all of the positive charged graphene have ionic bond with F^-. For appropriate BOE exposure time the effect of charge transfer doping between H_2O/O_2 and graphene can be eliminated (yielding the intrinsic state in Figure 3g).

Semi-ionic bonding between the graphene and F^- ions by the Coulomb force was difficult to permanently maintain because the positively charged graphene can be neutralized by receiving electrons from the negative ions[31,32] or the free electrons by γ rays[33] in air. The negative ions were produced by the nuclear radiation from either the radioactive minerals or radioactive gases, which are released from the earth's crust in air.[31,32] And the free electrons were produced by γ rays leaking from radioactive materials.[33] Further studies were needed to clarify the origin of the neutralization process of graphene in air. As the F^- ions were removed from the graphene (Supporting Information Figure S1 and S2), the graphene was again p-doped by the H_2O/O_2 redox system upon exposure to air. It means that, due to very small undercut of Si_3N_4 layer by BOE solution (0.78 nm, BOE treatment for 39 s) compared to the channel size of graphene (10 μm $\times$ 10 μm), most of the graphene regions in the devices treated by BOE solution were physically attached on Si_3N_4 and the electrical properties of graphene were directly affected by an underlying substrate containing O_2 solvated in a very thin water layer formed on Si_3N_4. Figure 4 shows the changes in the transfer characteristics, Dirac point, net charge density. and resistance of the GFET based on a Si_3N_4 gate insulator upon exposure to air. As the time of exposure to air increased, V_{dirac} in GFET was increasingly shifted to positive gate voltage (Figure 4a,b), and the resistance, R_{SD}, of the graphene layer between source and drain, obtained from the IV characteristics, gradually decreased (Figure 4c). In Figure 4b (right axis), the net charge density was estimated using, $n = (\varepsilon\varepsilon_0/d_s)\Delta V_{Dirac}$, where $\varepsilon = 7.5\varepsilon_0$ and $d_s = 100$ nm are the permittivity and thickness of the Si_3N_4 gate dielectric, respectively. The net charge density changed from zero to 1.8 $\times$ 10^{13} cm^{-2} during exposure in air after 18 days. In Figure 4b (blue line), the Dirac point and net charge density of PMMA-coated GFETs after BOE treatment changed from zero to 17.5 V and 6.6 $\times$ 10^{12} cm^{-2}, respectively. This indicates that the graphene layer is p-doped by the reaction between graphene and the H_2O/O_2 redox system and that the fluorine was detached from graphene. However, in the case of PMMA-coated GFETs, they were p-doped less than BOE-treated GFETs because PMMA evidently substantially deters the formation of the H_2O/O_2 redox system.

CONCLUSION

BOE recovers the intrinsic graphene. The dominant factor for p-doping of graphene is the interaction between the H_2O/O_2 redox system and graphene, as the V_{dirac} of the GFETs with the residual PMMA was $\sim$0 V. Exposure of the GFET to the BOE solution converts at least part of the H_2O layer into F^- and H_3O^+ ions, and the F^- ions have bonds with the graphene, removing the driving force for p-doping by removing the interaction between the H_2O/O_2 redox system and graphene. Upon re-exposure to air p-doping again occurs as the H_2O/O_2 redox system is again introduced between the graphene and the Si_3N_4 substrate. PMMA-coated graphene was less p-doped than graphene evidently because the PMMA layer restricts formation of as extensive an H_2O/O_2 redox system. The discovery that BOE can recover intrinsic graphene opens up new opportunities for its reliable application in nanoelectronics and optoelectronics.

EXPERIMENTAL SECTION

Graphene Synthesis Using CVD. Graphene was synthesized by thermal CVD. In the first step of synthesis, a roll of copper foil was inserted into a quartz tube and heated to 1000 °C (heating rate: 10 °C/min) with a flow of 10 sccm of H_2 at 1 Torr. The copper foils were heat-treated to increase the grain size for 30 min, as previously done.[34,35] For the synthesis of graphene, a gas mixture of CH_4 and H_2 was then flowed at 1 Torr for 30 min (1,000 °C) with rates of 20 and 10 sccm, respectively. Finally, the sample was cooled down to 300 °C (5 °C/s) under flowing H_2. The resulting graphene film on copper foil was spin-coated with PMMA, and the copper foil was etched in a plastic bath filled with ammonium persulphate solution, $(NH_4)_2S_2O_8$. The PMMA/graphene film was then transferred onto arbitrary substrates after being cleaned with deionized (DI) water for tens of minutes. PMMA was removed at least in part by washing with acetone.

Si_3N_4 Deposition and Etching Rate in BOE. To investigate the effect of the BOE treatment on back-gated GFETs, the GFETs were made on $\sim$100 nm thick Si_3N_4 that was deposited on a p^{++} Si substrate by low pressure chemical vapor deposition (LPCVD). A SiO_2 layer with a high etching rate of $\sim$100 nm/min[36] in BOE

(J. T. Baker, 6:1 volume ratio of 40% NH_4F in water to 49% HF in water) was not suitable in this experiment because the graphene layer easily peeled off. For the Si_3N_4, the BOE etching rate was about 1.2 nm/min. GFETs were not easily peeled off from the Si_3N_4 by a BOE treatment lasting tens of seconds.

Fabrication and Characterization of Graphene FET. Both conventional photolithography and e-beam evaporation were used to make Ti/Au electrodes (15 nm/50 nm) by drawing a photoresist (PR) line pattern onto the graphene regime that was selectively preserved. For a selective graphene etching, the PR pattern on the graphene was used as an etch mask. Graphene, except for the channel area and the electrode part, was etched away by O_2 plasma using a reactive ion etcher (RIE, Miniplasma-Cube, Plasmart) set at 100 W for 10 s. The GFET channel length was 10 μm and the width was 10 μm. All electrical transport characteristics were measured at room temperature with a source−drain (S−D) bias voltage of V_{ds} = 1 V in a probe station coupled to a semiconductor parameter analyzer (Keithley 4200). The Raman spectra of graphene on the Si_3N_4 substrates (82 nm thick) were measured with a micro-Raman system (Renishaw, RM1000-In Via) with laser excitation at 633 nm and a 50× objective lens, before and after BOE treatment. Samples of 1 cm × 1 cm (graphene on Si_3N_4/Si substrate) were measured by X-ray photoelectron spectroscopy (XPS, VG microtech ESCA 2000).

Conflict of Interest: The authors declare no competing financial interest.

Acknowledgment. This study was supported by the Basic Science Research Program through the National Research Foundation of Korea (NRF) funded by the Ministry of Education, Science and Technology (2011-0006268) and Samsung Mobile Display. R.S.R. is supported by SWAN-NRI, ONR, and the NSF of the USA and is a Distinguished Visiting Chair Professor, SAINT-SKKU.

Supporting Information Available: XPS spectra of graphene and Si_3N_4 dielectric layer before and after BOE treatment. This material is available free of charge *via* the Internet at http://pubs.acs.org.

REFERENCES AND NOTES

1. Schedin, F.; Geim, A. K.; Morozov, S. V.; Hill, E. W.; Blake, P.; Katsnelson, M. I.; Novoselov, K. S. Detection of Individual Gas Molecules Adsorbed on Graphene. *Nat. Mater.* **2007**, *6*, 652–655.
2. Chen, J.-H.; Jang, C.; Adam, S.; Fuhrer, M. S.; Williams, E. D.; Ishigami, M. Charged-Impurity Scattering in Graphene. *Nat. Phys.* **2008**, *4*, 377–381.
3. Lohmann, T.; von Klitzing, K.; Smet, J. H. Four-Terminal Magneto-Transport in Graphene p-n Junctions Created by Spatially Selective Doping. *Nano Lett.* **2009**, *9*, 1973–1979.
4. Farmer, D. B.; Golizadeh-Mojarad, R.; Perebeinos, V.; Lin, Y. M.; Tulevski, G. S.; Tsang, J. C.; Avouris, P. Chemical Doping and Electron-Hole Conduction Asymmetry in Graphene Devices. *Nano Lett.* **2009**, *9*, 388–392.
5. Dong, X.; Fu, D.; Fang, W.; Shi, Y.; Chen, P.; Li, L.-J. Doping Single-Layer Graphene with Aromatic Molecules. *Small* **2009**, *5*, 1422–1426.
6. Levesque, P. L.; Sabri, S. S.; Aguirre, C. M.; Guillemette, J.; Siaj, M.; Desjardins, P.; Szkopek, T.; Martel, R. Probing Charge Transfer at Surfaces Using Graphene Transistor. *Nano Lett.* **2011**, *11*, 132–137.
7. Ni, Z. H.; Wang, H. M.; Luo, Z. Q.; Wang, Y. Y.; Yu, T.; Wu, Y. H.; Shen, Z. X. The Effect of Vacuum Annealing on Graphene. *J. Raman Spectrosc.* **2010**, *41*, 479–483.
8. Dan, Y.; Lu, Y.; Kybert, N. J.; Luo, Z.; Johnson, A. T. C. Intrinsic Response of Graphene Vapor Sensors. *Nano Lett.* **2009**, *9*, 1472–1475.
9. Ishigami, M.; Chen, J. H.; Cullen, W. G.; Fuhrer, M. S.; Williams, E. D. Atomic Structure of Graphene on SiO_2. *Nano Lett.* **2007**, *7*, 1643–1648.
10. Dean, C. R.; Young, A. F.; Meric, I.; Lee, C.; Wang, L.; Sorgenfrei, S.; Watanabe, K.; Taniguchi, T.; Kim, P.; Shepard, K. L.; *et al.* Boron Nitride Substrates for High-Quality Graphene Electronics. *Nat. Nanotechnol.* **2010**, *5*, 722–726.
11. Cheng, Z.; Zhou, Q.; Wang, C.; Li, Q.; Wang, C.; Fang, Y. Toward Intrinsic Graphene Surfaces: A Systematic Study on Thermal Annealing and Wet-Chemical Treatment of SiO_2-Supported Graphene Devices. *Nano Lett.* **2011**, *11*, 767–771.
12. Collins, P. G.; Bradley, K.; Ishigami, M.; Zettl, A. Extreme Oxygen Sensitivity of Electronic Properties of Carbon Nanotubes. *Science* **2000**, *287*, 1801–1804.
13. Kim, W.; Javey, A.; Vermesh, O.; Wang, Q.; Li, Y.; Dai, H. Hysteresis Caused by Water Molecules in Carbon Nanotube Field-Effect Transistors. *Nano Lett.* **2003**, *3*, 193–198.
14. Aguirre, C. M.; Levesque, P. L.; Paillet, M.; Lapointe, F.; St-Antoine, B. C.; Desjardins, P.; Martel, R. The Role of The Oxygen/Water Redox Couple in Suppressing Electron Conduction in Field-Effect Transistors. *Adv. Mater.* **2009**, *21*, 3087–3091.
15. Bolotin, K. I.; Sikes, K. J.; Jiang, Z.; Klima, M.; Fudenberg, G.; Hone, J.; Kim, P. Stormer, H. L. Ultrahigh Electron Mobility in Suspended Graphene. *Solid State Commun.* **2008**, *146*, 351–355.
16. Zhang, H.; Bao, W.; Zhao, Z; Huang, J.-W.; Standley, B.; Liu, G.; Wang, F.; Kratz, P.; Jing, L.; Bockrath, M.; *et al.* Visualizing Electrical Breakdown and ON/OFF States in Electrically Switchable Suspended Graphene Break Junctions. *Nano Lett.* **2012**, *12*, 1772–1775.
17. Jung, I.; Pelton, M.; Piner, R.; Dikin, D. A.; Stankovich, S.; Watcharotone, S.; Hausner, M.; Ruoff, R. S. Simple Approach for High-Contrast Optical Imaging and Characterization of Graphene-Based Sheets. *Nano Lett.* **2007**, *7*, 3569–3575.
18. Gao, L.; Ren, W.; Le, F.; Cheng, H.-M. Total Color Difference for Rapid and Accurate Identification of Graphene. *ACS Nano* **2008**, *2*, 1625–1633.
19. Xia, X.; Tu, J.; Mai, Y.; Chen, R.; Wang, X.; Gu, C.; Zhao, X. Graphene Sheet/Porous NiO Hybrid Film for Supercapacitor Applications. *Chem.—Eur. J.* **2011**, *17*, 10898–10905.
20. Pirkle, A.; Chan, J.; Venugopal, A.; Hinojos, D.; Magnuson, C. W.; McDonnell, S.; Colombo, L.; Vogel, E. M.; Ruoff, R. S.; Wallace, R. M. The Effect of Chemical Residues on the Physical and Electrical Properties of Chemical Vapor Deposited Graphene Transferred to SiO_2. *Appl. Phys. Lett.* **2011**, *99*, 122108.
21. Jin, S.; Atrens, A. ESCA-Studies of the Structure and Composition of the Passive Film Formed on Stainless Steels by Various Immersion Times in 0.1 M NaCl Solution. *Appl. Phys. A: Mater. Sci. Process.* **1987**, *42*, 149–165.
22. Lim, A. S.; Atrens, A. ESCA Studies of Nitrogen-Containing Stainless Steels. *Appl. Phys. A: Mater. Sci. Process.* **1990**, *51*, 411–418.
23. Jones, C.; Sammann, E. The Effect of Low Power Plasmas on Carbon Fiber Surfaces. *Carbon* **1990**, *28*, 509–514.
24. Fubini, B.; Volante, M.; Bolis, V.; Giamello, E. Reactivity Towards Water of Silicon Nitride: Energy of Interaction and Hydration Dehydration Mechanism. *J. Mater. Sci.* **1989**, *24*, 549–556.
25. Nisar, J.; Araújo, M; Ahuja, R. Structural, Electronic and Energetic Properties of Water Adsorbed on β-Si_3N_4 (0001) Surface: First-Principles Calculations. *Surf. Sci.* **2010**, *604*, 617–622.
26. Park, Y.-B.; Rhee, S.-W. Optoelectronic Properties of Fluorine-Doped Silicon Nitride Thin Films. *J. Non-Cryst. Solids* **2004**, *343*, 33–38.
27. Nakajima, T.; Koh, M.; Gupta, V.; Žemva, B.; Lutar, K. Electrochemical Behavior of Graphite Highly Fluorinated by High Oxidation State Complex Fluorides and Elemental Fluorine. *Electrochim. Acta* **2000**, *45*, 1655–1661.
28. Chakrapani, V.; Angus, J. C.; Anderson, A. B.; Wolter, S. D.; Stoner, B. R.; Sumanasekera, G. U. Charge Transfer Equilibria Between Diamond and an Aqueous Oxygen Electrochemical Redox Couple. *Science* **2007**, *318*, 1424–1430.
29. Barone, V.; Hod, O.; Scuseria, G. Electronic Structure and Stability of Semiconducting Graphene Nanoribbons. *Nano Lett.* **2006**, *6*, 2748–2754.

30. Sawyer, D. *Oxygen Chemistry*; Oxford University Press: New York, 1991.
31. Laakso, L; Petäjä, T.; Lehtinen, K. E. J.; Kulmala, M.; Paatero, J.; Hõrrak, U.; Tammet, H.; Joutsensaari, J. Ion Production Rate in a Boreal Forest Based on Ion, Particle and Radiation Measurements. *Atmos. Chem. Phys.* **2004**, *4*, 1933–1943.
32. Chandrashekara, M. S.; Sannappa, J.; Paramesh, L. Studies on Atmospheric Electrical Conductivity Related to Radon and Its Progeny Concentrations in the Lower Atmosphere at Mysore. *Atmos. Environ.* **2006**, *40*, 87–95.
33. Dimant, Y. S.; Nusinovich, G. S.; Sprangle, P.; Penano, J.; Romero-Talamas, C. A.; Granatstein, V. L. Propagation of Gamma Rays and Production of Free Electrons in Air. 2012. e-Print archive. http://arxiv.org/abs/1204.2186.
34. Bae, S.; Kim, H.; Lee, Y.; Xu, X.; Park, J.-S.; Zheng, Yi.; Balakrishnan, J.; Lei, T.; Kim, H. R.; Song, Y. I.; *et al.* Roll-to-Roll Production of 30-Inch Graphene Films for Transparant Electrodes. *Nat. Nanotechnol.* **2010**, *5*, 574–578.
35. Li, X.; Cai, W.; An, J.; Kim, S.; Nah, J.; Yang, D.; Piner, R.; Velamakanni, A.; Jung, I.; Tutuc, E.; *et al.* Large-Area Synthesis of High-Quality and Uniform Graphene Films on Copper Foils. *Science* **2009**, *324*, 1312–1314.
36. Williams, K. R.; Muller, R. S. Etch Rates for Micromachining Processing. *J. Microelectromech. Syst.* **1996**, *5*, 256–269.